Molecular Modeling of the RNA Binding *N*-Terminal Part of Cowpea Chlorotic Mottle Virus Coat Protein in Solution with Phosphate Ions

David van der Spoel,* K. Anton Feenstra,# Marcus A. Hemminga,# and Herman J. C. Berendsen*
*Bioson Research Institute and Laboratory of Biophysical Chemistry, University of Groningen, 9747 AG Groningen, The Netherlands, and #Department of Molecular Physics, Agricultural University, 6700 ET Wageningen, The Netherlands

ABSTRACT The RNA-binding *N*-terminal arm of the coat protein of cowpea chlorotic mottle virus has been studied with five molecular dynamics simulations of 2.0 ns each. This 25-residue peptide (pep25) is highly charged: it contains six Arg and three Lys residues. An α-helical fraction of the sequence is stabilized in vitro by salts. The interaction of monophosphate (Pi) ions with pep25 was studied, and it was found that only two Pi ions are bound to pep25 on average, but water-mediated interactions between pep25 and Pi, which provide electrostatic screening for intrapeptide interactions, are abundant. Shielding by the Pi ions of repulsive electrostatic interactions between Arg sidechains increases the α-helicity of pep25. A hydrogen bond at the *N*-terminal end of the α-helix renders extension of the α-helix in the *N*-terminal direction impossible, in agreement with evidence from nuclear magnetic resonance experiments.

INTRODUCTION

Cowpea chlorotic mottle virus (CCMV) is a spherical plant virus of the group of bromoviruses. It consists of ribonucleic acid (RNA) surrounded by 180 identical, icosahedrally arranged protein subunits (Dasgupta and Kaesberg, 1982). The virus particle can easily be dissociated and reassembled in vitro by changing pH and ionic strength (Bancroft and Hiebert, 1967). The highly positively charged *N*-terminal arm (six Arg and three Lys) consisting of the first 25 amino acids of the coat protein has been found to be essential for binding the encapsulated RNA (Vriend et al., 1981). Based on nuclear magnetic resonance (NMR) experiments and secondary structure predictions, Vriend et al. (1982, 1986) proposed a "snatch-pull" model for the assembly of CCMV coat protein and RNA. In this model the *N*-terminal region of the coat protein changes from a random coil conformation into an α-helical conformation located between Arg-10 and Asn-20 on binding viral RNA. Chemical synthesis of the pentacosapeptide pep25 that contains the first 25 *N*-terminal amino acids of CCMV coat protein (ten Kortenaar et al., 1986) permitted detailed spectroscopic studies to test the snatch-pull model. Circular dichroism experiments showed that addition of inorganic salts to pep25 results in an increase of α-helix content, especially in the presence of octadecaphosphate (van der Graaf and Hemminga, 1991). A two-dimensional ^{1}H-NMR study of pep25 indicated the presence of a conformational ensemble consisting of helical structures rapidly converting into more-extended states (van der Graaf et al., 1991). The helical region is found to be situated between Thr-9 and Ala-17, which agrees remarkably well with the secondary-structure predictions (Vriend et al., 1986, 1982). This NMR work has been extended by distance geometry calculations of pep25 in the presence of tetraphosphate (Pi4) (van der Graaf et al., 1992), which yielded eight structures belonging to two structure families. The first family consists of five structures with an α-helix-like conformation in the middle of the peptide, and the second family consists of three structures with a more open conformation. Although the occurrence of two structure families suggests that even in the presence of Pi4 the peptide is flexible, its tendency to form an α-helical conformation on binding of phosphate groups is suggested to play an essential role in RNA binding (van der Graaf et al., 1992).

It is well known that changes in the environment of a polypeptide chain can induce changes in the conformation (Timasheff, 1992), for example, the unfolding of proteins induced by urea (Sijpkes et al., 1993) or the promotion of α-helix content by alcohols (Brooks and Nilsson, 1993) or phosphate ions (van der Graaf and Hemminga, 1991). The precise mechanism of the action is not known; therefore it is interesting to study the binding of small molecules to polypeptides. Theoretical methods such as molecular dynamics (MD) simulations are very attractive tools for these studies because they can give atomic detail on a time scale (nanoseconds) that is relevant for the motion of these small molecules. MD simulations were used previously to study the influence of trifluoroethanol and other alcohols on the structure of peptides (de Loof et al., 1992; van Buuren and Berendsen, 1993; Brooks and Nilsson, 1993; Kovacs et al., 1995), and simulations of protein unfolding are quite common (Mark and van Gunsteren, 1992; Brooks, 1993; Tirado-Rives and Jorgensen, 1993; Caflisch and Karplus, 1994). The effect of salts on the structure of peptides has also been studied by simulation techniques (Smith and Pettitt, 1991b; Smith et al., 1993). Refinement of protein structures based on NMR or x-ray data is a very important application of MD, and many methodological improvements are still being developed (van Schaik et al., 1993; Clarage and Philips, 1994; Fennen et al., 1995). In the context of structure

Received for publication 16 April 1996 and in final form 28 August 1996.
Address reprint requests to Dr. H. J. C. Berendsen, Department of Chemistry, University of Groningen, Nijenborgh 4, 9747 AG Groningen, The Netherlands. Tel.: 31-50-3634327; Fax: 31-50-3634800; E-mail: berends@chem.rug.nl.
© 1996 by the Biophysical Society
0006-3495/96/12/2920/13 $2.00

determination, pep25 is a very challenging case: there is a large amount of experimental data from NMR and circular dichroism (CD) spectroscopy, but the structure is not known in atomic detail. The conformation of pep25 is influenced by the addition of phosphate ions; both concentration and chemical composition of the phosphate molecules are important for the structure of pep25 (van der Graaf et al., 1991). It is important to note that α-helical structure is induced in pep25 not only by neutralization or shielding of the charged residues but also by specific interaction of phosphate groups with the peptide. Experimental results have shown that in the presence of phosphates the α-helix content is slightly larger than with other salts and that the use of longer phosphate chains, resembling RNA, drastically increased the α-helicity (van der Graaf et al., 1991).

Here we have attempted to model pep25 by simulations in the presence of monophosphate (Pi) ions. The questions that we will address are the following: 1) Where do phosphate ions bind to the peptide? 2) Which part of the peptide is α-helical in the presence of phosphates? 3) How stable is the α-helix in the simulation? 4) Why does the α-helix not extend in the *N*-terminal direction from Arg-10?

We will emphasize the comparison of simulation data with experimental data, such as $^1H_\alpha$ chemical shifts and α-helicity (corresponding to ellipticity from CD measurements). For comparison, we also performed simulations of pep25 without counterions and of pep25 in the presence of a Pi4 molecule and in the presence of a Pi8 molecule, although these simulations suffer from methodological problems, in particular in the treatment of electrostatic interactions (Smith and Pettitt, 1991a) and in the limited sampling of phase space.

METHODS

Starting structure for pep25

The peptide pep25 resembles the *N*-terminal arm of the CCMV coat protein; its sequence is given in Table 1. As a starting structure for our simulations we used the distance geometry structure with the largest number of α-helical residues (structure 3 of van der Graaf et al. (1992)).

Docking phosphate on pep25

The usual procedure for placing ions around a polypeptide chain for MD simulation is first to solvate the protein and subsequently to replace water molecules by ions at the positions that are energetically most favorable. Because this procedure does not work for large ions such as Pi, we employed another method. We obtained the starting conformations for the MD simulations with phosphate by performing vacuum MD simulations in which pep25 was surrounded by randomly distributed phosphate molecules. To avoid immediate clustering of the phosphate molecules on the charged sidechains of pep25 owing to the omission of explicit water molecules we used a relative dielectric constant ϵ_r of 4 to reduce the strength of the Coulomb interactions. The peptide was harmonically restrained to its starting conformation with a force constant of 1000 kJ mol^{-1} nm^{-2} to conserve its structure. The simulations were performed at constant temperature by weak coupling to a temperature bath at 300 K with a coupling constant of 0.1 ps (Berendsen et al., 1984). The time step was 1 fs in all vacuum simulations. All bonds were constrained to their equilibrium length by the SHAKE algorithm (Ryckaert et al., 1977). The simulations were performed with the GROMACS software package (van der Spoel et al., 1996; Berendsen et al., 1995) on a Silicon Graphics Indy workstation.

A single vacuum run with p25 and nine randomly distributed Pi molecules was performed for 25 ps. The starting conformation for the monophosphate run is the last frame from this simulation, which seemed to have a reasonable distribution of Pi molecules around pep25 and in solution, as judged by visual inspection. We refer to the simulation from this starting conformation as Sim 9Pi-D (where D means docked). To test what influence the starting conformation has on the distribution of the Pi ions during the simulation, we generated an extra starting conformation, using the same peptide structure and nine randomly placed Pi ions without docking. We refer to the simulation from this starting conformation as Sim 9Pi-R (where R means random).

Ten separate vacuum runs with p25 and three randomly distributed Pi4 molecules were performed for 100 ps. Because of the high charge on the Pi4 molecules and the lower mobility of Pi4 relative to Pi because of the larger size, clustering is a more serious problem than with Pi; therefore multiple docking simulations had to be performed. We overlaid the last time frame of all 10 simulations to see whether Pi4 clusters to the peptide in specific positions along the sequence. Then one of these frames that had all three Pi4 molecules in or close to a different phosphate cluster was selected. From this conformation two Pi4 molecules were deleted, leaving the phosphate closest to Arg-10, -13, -14 and -18. To keep things simple for Pi8, we manually docked one Pi8 at approximately the same position that Pi4 has in the starting conformation described above, using the Quanta software package (MSI, 1994). We refer to the simulations with these large phosphate chains as Sim Pi4 and Sim Pi8, respectively.

Solvation of peptides

For the simulation of pep25 in aqueous solution the peptide was solvated in a box of simple point charge water (Berendsen et al., 1981) large enough to accommodate the peptide (approximately 4.8 × 4.8 × 4.8 nm). We built this water box by stacking cubic boxes containing 216 equilibrated water molecules. All water molecules within 0.23 nm of a peptide atom were removed. For the simulations of pep25 with phosphate ions, the phosphate

TABLE 1 Amino acid sequence of pep25, resembling the *N*-terminal arm of the CCMV coat protein (Dasgupta and Kaesberg, 1982)

	OH	OH			OH		+		OH	+		ON	+	+	
Ac	Ser	Thr	Val	Gly	Thr	Gly	Lys	Leu	Thr	Arg	Ala	Gln	Arg	Arg	Ala
	1				5					10					15
			+	+	ON	+	+	ON	OH	+					
	Ala	Ala	Arg	Lys	Asn	Lys	Arg	Asn	Thr	Arg	Nac				
					20					25					

The Nac residue at the *C*-terminus is an $NHCH_3$ group that is present in the chemically synthesized peptide (ten Kortenaar et al., 1986). Indicated are charged groups (+) and hydrogen-bond forming sidechains. OH is the OH group and ON is the $CONH_2$ group.

TABLE 2 Number of atoms in each simulation

	Sim W	Sim 9Pi-D/R	Sim Pi4	Sim Pi8
pep25	276	276	276	276
Phosphate		63(9Pi)	19(Pi4)	35(Pi8)
H_2O	10050	9792	8682	9972
Total	10326	10131	8977	10283

molecules were placed in the box with pep25 as described above before the peptide–ion complex was dissolved. The solvation procedure was then the same as in the run without ions. The total number of atoms in each simulation is given in Table 2. All five starting structures were then subjected to energy minimizations by the steepest-descents method. During minimization the peptide was harmonically restrained with a force constant of 1000 kJ mol^{-1} nm^{-2}. A cutoff for electrostatic interactions of 1.8 nm was used in the energy minimizations. The final structures were used as starting conformations for the production MD runs.

Force field for phosphate ions

In the GROMOS87 force field (van Gunsteren and Berendsen, 1987) no complete parameter set for the phosphate ions is available. Therefore we decided to use the Lennard–Jones parameters as well as the force constants for angle bending and dihedral angle torsions from GROMOS87 and to determine the charges and geometries from ab initio calculations. We did a full geometry optimization of Pi ($H_2PO_4^-$) with the 6-31++G** basis set, using the Gaussian-92 package (Frisch et al., 1993). Symmetry was not taken into account during the calculation. Subsequently we derived the atomic charges for the Pi molecule. The Merz–Kollman population analysis, which fits the charges to the molecular electrostatic potential (Besler et al., 1990), was used with the included solvent reaction field as implemented in Gaussian-92. The computation was done with a dielectric constant of 78.5 and a cavity radius of 0.358 nm. We imposed exact symmetry afterward by assigning average charges, bond lengths, and angles to symmetrically identical atoms or bonds. The resulting parameters are listed in Table 3. The charges are almost 50% higher than those of Lee and Prohofsky (1982), probably because of the inclusion of the solvent reaction field.

A full geometry optimization of Pi4 ($H_3P_4O_{13}^-$) was done with the 3-21G basis-set, followed by a Merz–Kollman population analysis with cavity radius of 0.475 nm. A smaller basis set than for Pi was used because of the larger system size (19 atoms). The force constants for the angles OA–P–OA (Pi) and OA–P–OS (Pi4) are taken to be the same as those for all O–P–O angles, except OM–P–OM, consistent with the GROMOS87 force field. The parameters are listed in Table 4.

The geometry of Pi8 ($H_2P_8O_{25}^{8-}$) was not determined by ab initio calculations; instead we copied it from Pi4 because of the large system size (35 atoms) and because no large deviations from Pi4 were expected. In effect, each of the two middle PO_3 groups was copied twice and inserted between its original position and the central oxygen atom. The charge distribution on Pi8 was again calculated by a Merz–Kollman population analysis with a cavity radius of 0.579 nm. The charges are listed in Table 5. A plot of the phosphate molecules is given in Fig. 1.

Molecular dynamics

Five MD simulations of pep25 in water were performed. Sim W had no counterions, Sim 9Pi-D had nine Pi molecules starting from a docking simulation in vacuum as described above, Sim 9Pi-R also had nine Pi ions starting from random positions, Sim Pi4 had one Pi4 ion, and Sim Pi8 had one Pi8 ion. The GROMOS force field (van Gunsteren and Berendsen, 1987) was used, with increased repulsion between water oxygen and carbon atoms, as suggested by Van Buuren et al. (1993); the resulting parameter set is the one referred to as SW by Daura et al. (1996). Each simulation was 2.0 ns, with a time step of 2 fs. SHAKE (Ryckaert et al., 1977) was used for all bonds. A twin-range cutoff for nonbonded interactions was employed, with short-range cutoff for Van der Waals and Coulomb interactions of 1.0 nm and a long-range cutoff of 1.8 nm for Coulomb interactions that were calculated during neighbor-list generation, every 20 fs. Sim W and Sim 9Pi-D were actually performed twice, the first time with a single cutoff of 1.0 nm and the second time as indicated above. Because of the 1.0-nm cutoff the first simulations were not reliable, as is explained in the Results section. Therefore we used only the simulations with 1.8-nm long-range interactions for our analysis. The temperature was controlled by weak coupling to a bath of 300 K (Berendsen et al., 1984) with a time constant of 0.1 ps. Protein and solvent (including phosphate where appropriate) were coupled to the heat bath independently. The pressure was also controlled by weak coupling with a time constant of 1.0 ps. Unlike in the vacuum simulations, no shielding of electrostatic interactions was performed because we used a relative dielectric constant ϵ_r of 1.

The MD simulations were carried out with the GROMACS software package (van der Spoel et al., 1996) on custom-built parallel computers (Bekker et al., 1993; Berendsen et al., 1995) with Intel i860 CPUs and on a Silicon Graphics Power Challenge. On our fastest parallel computer with 28 processors the 2.0-ns simulation of pep25 in water (10,326 particles) with parameters as stated above took 8.6 days of computer time.

Calculation of chemical shifts

To be able to compare our simulation data with experimental data we needed a method to compute chemical shifts from a structure. For this purpose we used the empirical method of Williamson and Asakura (1993). Recently there has been considerable progress in the computation of chemical shifts from structural data (Spera and Bax, 1991; Osapay and Case, 1991, 1994; Williamson and Asakura, 1993; Case, 1995). Although there has been impressive progress in the ab initio–based methods (Pearson et al., 1995; de Dios et al., 1995) those methods are not practical for our purpose: we want to average the chemical shift over our trajectory of 4000 frames, so the computation time must be short. The Williamson–Asakura method actually calculates the δ value; thus we had to subtract random coil values from the experimental data to be able to compare the data. For this purpose we used both the recently published values of Merutka et al.

TABLE 3 Charges and geometry of Pi

Atom	q (e)	Atoms	b_0 (nm)	k_b	Atoms	θ_0 (°)	k_θ
P	1.596	P–OM	0.1478	376560	OM–P–OM	124.8	585.76
OM	−0.943	P–OA	0.1637	251040	OM1–P–OA	105.9	397.48
OA	−0.777	OA–H	0.0943	313800	OM2–P–OA	108.2	397.48
HO	0.422				P–OA–H	108.2	397.48
					OA–P–OA	101.5	400

OA is the alcohol oxygen and OM is the "charged" oxygen (these names correspond to the GROMOS atom types). The two OM atoms have different angles from the OA atoms. Dihedral parameters (*H-OA-P-OA*) were taken from GROMOS. b_0 is the bond length, θ_0 is the bond angle, k_b is the force constant for bond stretching (in kJ mol^{-1} nm^{-2}), and k_θ is the force constant for angle bending (in kJ mol^{-1} rad^{-2}).

TABLE 4 Charges and geometry of Pi4

Atom	q (e)	Atoms	θ_0 (°)	k_θ	Atoms	b_0 (nm)	k_b	Atoms	ϕ_0 (°)	k_ϕ	n_ϕ
P1	1.85	OA–P–OS	97	400	P–OM	0.155	376560	H–OA–P–OS	34	3.0	3
P2	1.95	OS–P–OS	102	397.48	P–OS	0.165	251040	OA–P–OS–P	−19	3.0	3
OM	−1.0	OS–P–OM	109	397.48	P–OA	0.164	251040	OS–P–OS–P	−222/−147	3.0	3
OS1	−0.92	OA–P–OM	110	397.48	OA–H	0.101	313800				
OS2	−0.88	P–OA–H	113	397.48							
OA	−1.02	OM–P–OM	118	585.76							
HO	0.58	P1–OS1–P2	137	397.48							
		P2–OS2–P2	147	397.48							

OA is the alcohol oxygen, OM is the "charged" oxygen, OS is the ether oxygen (these names correspond to the GROMOS atomtypes). Counting from the central ether oxygen (OS), the OS–P–OS–P dihedral angles are 147 and 222 alternatingly. The parameter b_0 is the bond length, θ_0 is the bond angle, ϕ_0 is the dihedral angle, k_b is the force constant for bond stretching (in kJ mol^{-1} nm^{-2}), k_θ is the force constant for angle bending (in kJ mol^{-1} rad^{-2}), k_ϕ is the force constant for the torsion potential (in kJ mol^{-1}), the multiplicity n_ϕ in the dihedral potential is the number of minima in the potential on the interval of 0 to 360°.

(1995) and the old standard of Bundi and Wüthrich (1979), although the differences for Hα protons are not large.

RESULTS

Long MD simulations, such as those presented here, produce great amounts of data to be analyzed. Some properties can be averaged over the trajectory or over part of the trajectory and compared with equilibrium properties from experiments. Examples of these properties are chemical shifts and radial distribution functions. Other properties, such as the binding of phosphate molecules to the peptide and dynamic changes in conformation, are interesting when dynamic information is analyzed. Most properties, however, can be viewed in both ways: for example, the formation and breaking of a hydrogen bond or a salt bridge is a dynamic process; the radial distribution function is an average property. We will analyze a number of the properties that can be deduced from the simulations that we have performed. It should be noted here that average properties are meaningful only when the trajectory represents an equilibrium ensemble. Most peptides in solution do not have a well-defined conformation; in other words, an ensemble of many configurations is present in a peptide solution. We do not pretend to find all possible conformations or even the most important conformations (with lowest free energy) in a 2.0-ns simulation of a single peptide.

TABLE 5 Charges on the Pi8 molecule

Atom	q (e)
P1	1.85
P2	1.95
P3	1.79
OM	−1.00
OS1	−0.88
OS2	−0.82
OS3	−0.76
OA	−1.05
HO	0.58

OA is the alcohol oxygen, OM is the "charged" oxygen, OS is the ether oxygen; these names correspond to the GROMOS atomtypes. Bond lengths, angles, dihedrals, and force constants are taken from the Pi4 geometry (see Table 4).

Nevertheless, we can calculate a number of average properties from the simulation trajectories. Comparison with experimental data should then point out whether (part of) the simulation data is physically meaningful.

α-Helicity

The first quantity that we analyzed is the α-helicity, which corresponds to the ellipticity at 222 nm as measured by CD experiments. The α-helicity is computed from Ramachandran angles according to a formula of Hirst and Brooks (1994). We plotted the fraction of time during which each residue is in an α-helical conformation in Sim W, Sim 9Pi-D, and Sim 9Pi-R (Fig. 2). The α-helix from residue 11-16 is present for more than 60% of the time in Sim 9Pi-D. The smaller peak around Gly-4 in Sim 9Pi-D and the single peak at Lys-21 can be explained by single residues' having α-helical ϕ/ψ angles rather than a local α-helical conformation of the peptide. In pure water (Sim W) the α-helix is not so pronounced as in Sim 9Pi-D; especially notable is the dip at Arg-14. The peak at Lys-21 is missing, but in the *N*-terminal part, around Thr-5, a small peak is present. The curve for Sim 9Pi-R resembles that of Sim W in the α-helical region, with a notable dip at Arg-14 and, in contrast to Sim 9Pi-D and Sim W, a peak at Arg-22. When averaged over the whole peptide and over time, pep25 has 6 α-helical residues in Sim 9Pi-D, 5 in Sim W, and 4.3 in Sim 9Pi-R. It is important to note that the ellipticity at 222 nm, as obtained from CD experiments, is an average over all ϕ/ψ angles, so it can be compared with our calculated averages. In Table 6 we have listed the averages. Although we cannot prove that our simulation represents an equilibrium ensemble, the correspondence between experiment and Sim 9Pi-D is striking.

$^1H_\alpha$ Chemical shifts

$^1H_\alpha$ chemical shifts have been measured for pep25 in the presence of different phosphates (van der Graaf et al., 1992). The most striking feature of the δ values (difference from random coil values) when they are plotted as a func

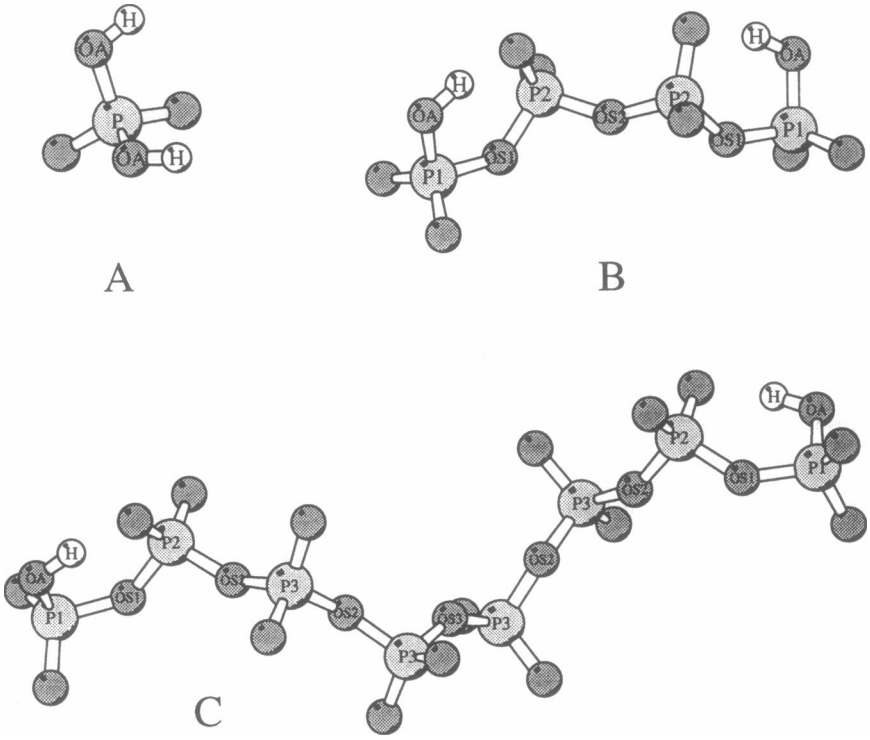

FIGURE 1 The Pi (*A*), Pi4 (*B*), and Pi8 (*C*) molecules. The plot was made with MOLSCRIPT (Kraulis, 1991).

tion of residue number is the sharp decrease at Arg-10 followed by a slow increase to values near 0 ppm (Fig. 3). The sharp decrease at Arg-10 has been interpreted (together with nuclear Overhauser–effect data) as the start of the α-helical region of pep25. We calculated the $^1H_\alpha$ chemical shifts from our trajectories of Sim 9Pi-D and Sim 9Pi-R, using the method of Willamson and Asakura (1993), and averaged the shifts over time (Fig. 3). The shifts calculated as an average over Sim 9Pi-D closely follow the experimental pattern; the trend from Ala-17 to Thr-24 is qualitatively reproduced. The sharp decrease in δ near Arg-10 is not so clear in Sim 9Pi-D as in the experimental data, and it seems to be shifted by one residue to Ala-11. In Sim 9Pi-R the peak at Leu-8 is reproduced quantitatively, but some large deviations near Ala-15 are visible as well. In the *N*-terminal part of the peptide there is a significant difference between experiment and both Sim 9Pi-D and Sim

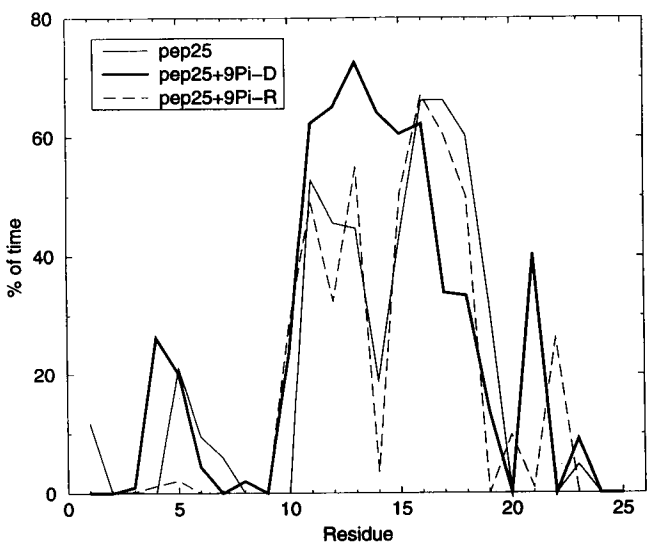

FIGURE 2 α-Helicity of all residues of pep25 averaged over time in Sim W and Sim 9Pi-D, according to the criterion of Hirst and Brooks (1994).

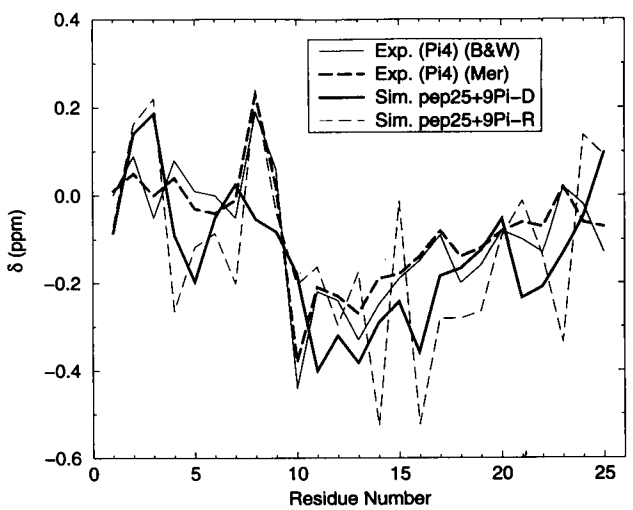

FIGURE 3 Conformational Cα-H chemical shifts measured by NMR in the presence of Pi4 (van der Graaf et al., 1992) and calculated from Sim 9Pi-D and Sim 9Pi-R by the empirical method of Williamson and Asakura (1993). (*Mer*) Random coil values of Merutka et al. (1995), (*B&W*) Random coil values of Bundi and Wüthrich (1979).

TABLE 6 Average α-helicity in Sim 9Pi-D/R and Sim W compared with values from CD spectroscopy (van der Graaf and Hemminga, 1991)

MD		CD	
Sim W	20 ± 3%	No salt	21.0%
Sim 9Pi-D	24 ± 3%	50 mM Pi	23.6%
Sim 9Pi-R	18 ± 3%		

9Pi-R. Because the experimental shifts are very close to random coil values, this suggests that some residual structure is present in pep25 during the simulations, which is not observed experimentally.

Conformation of pep25 in the simulations

Snapshots from the trajectories of Sim W, Sim 9Pi-D, and Sim 9Pi-R are plotted in Fig. 4 (Sim Pi4 and Sim Pi8 are not shown). In all simulations the starting conformation of pep25 is the same. The starting positions of the Pi ions are clearly different in Sim 9Pi-D and Sim 9Pi-R; in the former most ions are indeed docked on the peptide. The Arg residues in the α-helical region are pointing out of the plane of the paper.

After 1000 ps in Sim W the *N*- and *C*-terminal ends of pep25 have begun to collapse on top of the α-helical region, a process that continues until the end of the simulation. After 2000 ps the backbone is curled up, and all charged residues are pointing outward. Strangely, the α-helix seems not to be affected to a large degree, and a fair amount of α-helix is present in the end structure of Sim W. In Sim 9Pi-D four of the Pi molecules are initially located close to the α-helical region. The peptide seems to behave more as one would intuitively expect: it stretches (at 1000 ps) and then contracts again (2000 ps). The Pi ions are swarming around pep25; they seem not at all tightly bound. In both Sim 9Pi-D and Sim 9Pi-R the α-helix deforms somewhat, but the final structures are still more-or-less α-helical.

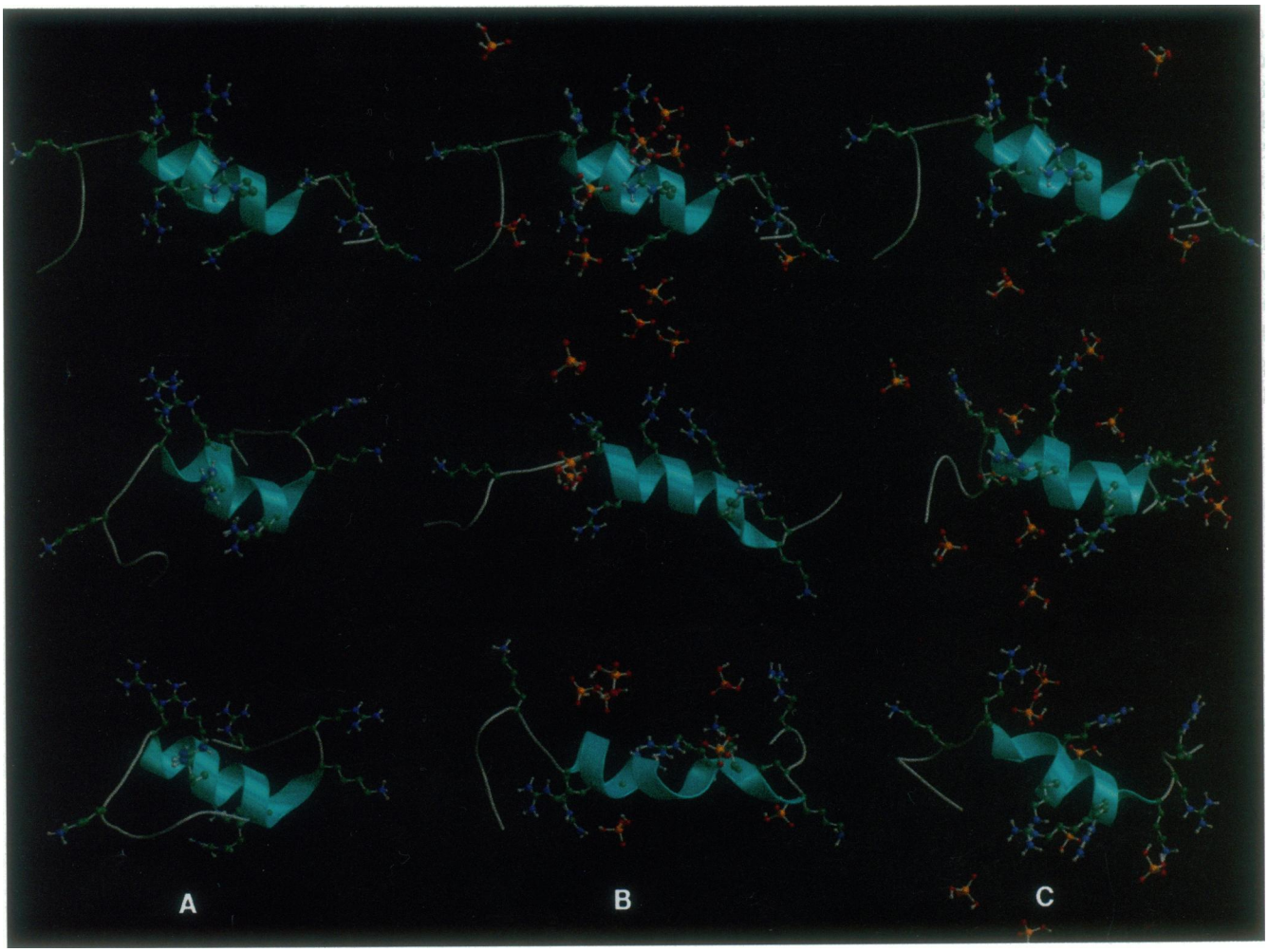

FIGURE 4 p25 Molecules at (*top to bottom*) $t = 0$, $t = 1000$ ps, and $t = 2000$ ps in (*A*) Sim W, (*B*) Sim 9Pi-D, (*C*) Sim 9Pi-R. The peptides were rotated such that the Arg residues are pointing out of the plane. Plots were made with MOLSCRIPT (Kraulis, 1991) and Raster3D (Bacon and Anderson, 1988; Merritt and Murphy, 1994).

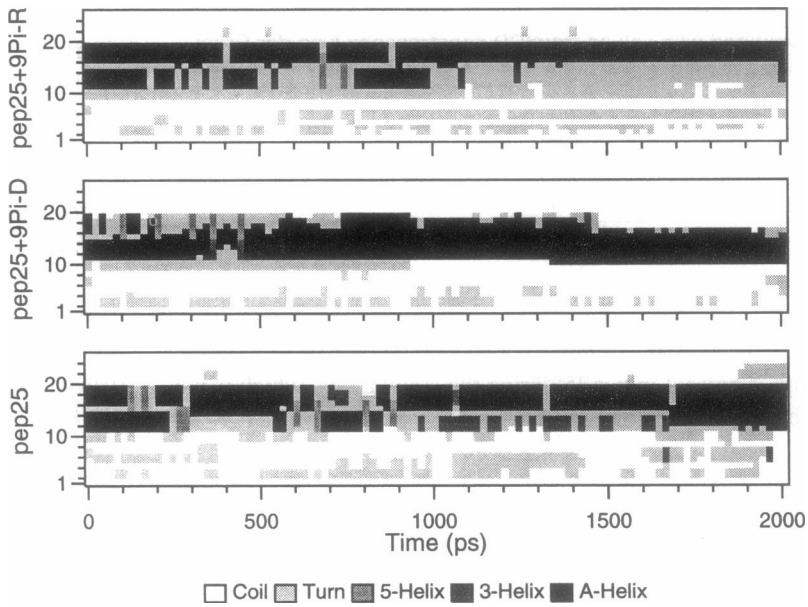

FIGURE 5 Secondary structure of pep25 in Sim W, Sim 9Pi-D, and Sim 9Pi-R.

Secondary structure

A revealing view of a protein or peptide simulation is a plot of the secondary structure as a function of time. In Fig. 5 we have plotted the secondary structure, calculated by the DSSP program (Kabsch and Sander, 1983). We see that in Sim W the peptide is α-helical from residue 11-20, with a single residue in the middle (Ala-15) that is not α-helical. After 250 ps the *N*-terminal part of the α-helix unfolds; in the rest of the simulations residues 11-14 alternate among α-helix, 3_{10}-helix, and π-helix. From ~1800 ps the α-helix is complete, with a length of nine residues (t = 2000 ps). During the whole simulation the *N*-terminal part of the peptide forms many hydrogen-bonded turns. In Sim 9Pi-D the α-helical region of the peptide alternates among π-helix, 3_{10}-helix, and α-helix, where the *C*-terminal end is less stable than the *N*-terminal end. After 500 ps, however, the α-helix is rather stable, and it remains so for the rest of the simulation, with little structure in the rest of the peptide. From 0 through 1320 ps the α-helix starts at Ala-11, but from 1340 to 2000 ps it starts at Arg-10. The peptide in Sim 9Pi-R behaves similarly to the one in Sim W, with the *C*-terminal end being very stable and the *N*-terminal end being α-helical primarily in the first half of the simulation.

Binding of Pi to pep25

We have analyzed the binding of Pi molecules to pep25 in detail. In Fig. 6 we have plotted the distance from each

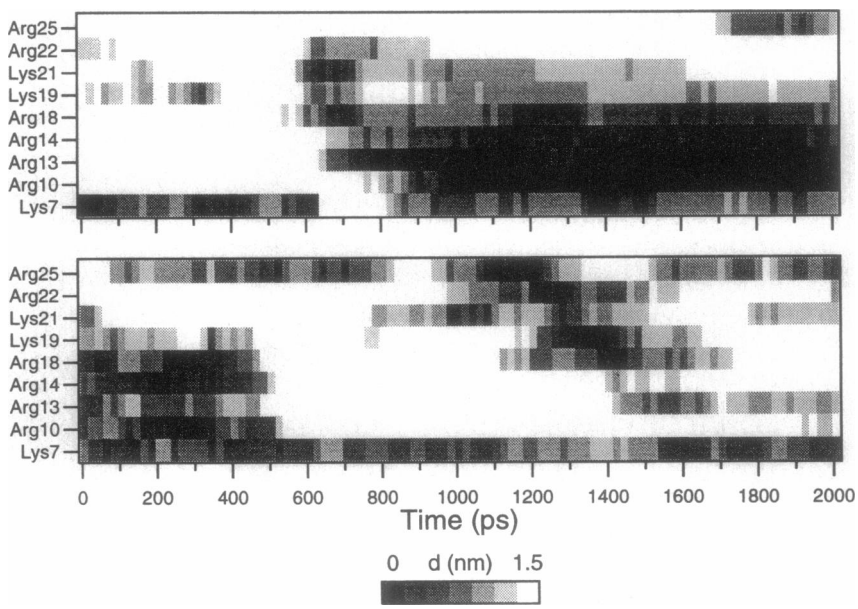

FIGURE 6 Smallest distance between any Pi atom to any atom of a charged sidechain of pep25 in Sim 9Pi-D (*bottom*) and Sim 9Pi-R (*top*).

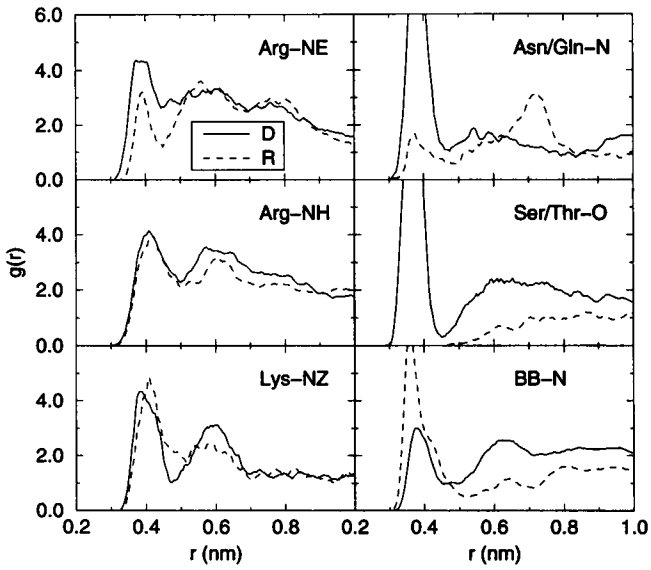

FIGURE 7 Radial distribution function of Pi-P atoms around sidechain and backbone proton donors. The central particles over which the RDF was averaged are denoted in the graphs. A running average over 0.025 nm was used to enhance clarity.

charged residue to the closest Pi molecule, calculated as the smallest distance from any Pi atom to any atom of the charged groups in the peptide (NZ + protons for Lys and NE, CZ, NH1, NH2 + protons for Arg). Thus the darkest areas in the figure indicate direct hydrogen bonding and one shade of gray lighter corresponds to water-mediated interactions. Initially the Pi molecules are distributed rather evenly around pep25 in Sim 9Pi-D, whereas they are far away in Sim 9Pi-R, except for a direct hydrogen bond with Lys-7. During the simulations the distribution of Pi molecules changes; in Sim 9Pi-D the Pi molecules dissolve after 500 ps, only to come back later on in the simulation; only Lys-7 is close to a Pi all the time. The Pi ions in Sim 9Pi-R find pep25 after 700 ps, and from that time on the ions are constantly close to the most-charged residues.

At a more detailed level, a radial distribution function (RDF) can give information about the environment of individual atoms; it can be used to study hydrogen bonding, salt bridges, and liquid structure in general (Allen and Tildesley, 1987). The RDF is defined as the local density of a certain group of particles around a central particle, and it can be averaged over multiple central particles. In Fig. 7 we have plotted the radial distribution of phosphorus atoms around proton donor groups in pep25. For the central particles we used the proton donor atoms rather than the hydrogen atoms to reduce noise from small fluctuations. The peak around the neutral groups of Ser/Thr and Asn/Gln is much higher than the one around any of the other groups in Sim 9Pi-D, but this is not so for Sim 9Pi-R. From this we can conclude two things: the Pi ions starting from random positions do not find the neutral groups, and, once Pi binds to these groups, it binds tightly. The Arg and Lys RDF plots are very similar in Sim 9Pi-D and Sim 9Pi-R, indicating that the long-range electrostatic interactions are strong enough to attract the Pi ions from their random starting positions in Sim 9Pi-R. The graphs also show a pronounced second peak, which may be due to neighboring residues but also to water-mediated hydrogen bonds.

Some special hydrogen-bond configurations between pep25 and Pi molecules are plotted in Fig. 8. An extended hydrogen-bonding network occurs among Arg-10, Arg-14, and a Pi molecule. Triple hydrogen bonding occurs for Lys-7, Arg-14, Lys-19, and Pi. Although double hydrogen bonds are not particularly abundant, bifurcated hydrogen bonds (one acceptor and two donors or vice versa) can be found quite frequently. The average number of pep25-Pi hydrogen bonds, including multiple hydrogen bonds with one residue, is 4.6 for Sim 9Pi-D and 3.9 for Sim 9Pi-R; the average number of Pi ions that are hydrogen bonded to pep25 is 2.3 for Sim 9Pi-D and 1.3 for Sim 9Pi-R. We see from this that every Pi that is bound to pep25 makes, on average, two hydrogen bonds with it in Sim 9Pi-D and three hydrogen bonds in Sim 9Pi-R.

Hydrogen bonding involving Thr-9

The hydrogen-bonding network around Thr-9 deserves special attention because Thr-9 is one of the key residues in the snatch-pull model for RNA binding (Vriend et al., 1986). Hydrogen bonds from backbone as well as from the sidechain of Gln-12 to the Thr-9 sidechain occur in Sim 9Pi-D. A simultaneous hydrogen bond of the Gln-12 sidechain to the Lys-7 backbone further stabilizes this hydrogen-bond network. Although this network is found only at the very end of the simulation (1900–2000 ps), we did also observe a hydrogen bond between Gln-12–NH and Thr-9–Oγ (1300–2000 ps). For the rest of the simulation the amino group of the Gln-12 side chain is hydrogen bonded to its own backbone atoms or to those of residues further back in the sequence (Leu-8–O, Lys-7–O, Thr-5–O). Gln-12–Oϵ1 is hydrogen bonded to its own backbone, NH, or to other backbone and sidechain atoms (Arg-13–NH1, Arg-13–NH2, Ala-17–NH). Hydrogen bonds are also observed between the backbones of Leu-8 and Gln-12 from 0 to 800 ps and of Thr-9 and Arg-13 from 1300 to 2000 ps. In effect, the latter hydrogen bond implies an extension of the α-helical conformation towards the *N*-terminus.

Charge–charge interactions

In Sim 9Pi-D we have not only the attractive interactions between Pi and peptide but also repulsive interactions between Pi molecules mutually and between charged sidechains of Lys and Arg residues. These interactions can cause problems when they are simulated with a cutoff radius. What typically happens is that two charges of the same sign repel each other until the distance is larger than the cutoff. After that, both charges diffuse randomly until the distance again becomes smaller than the cutoff. When

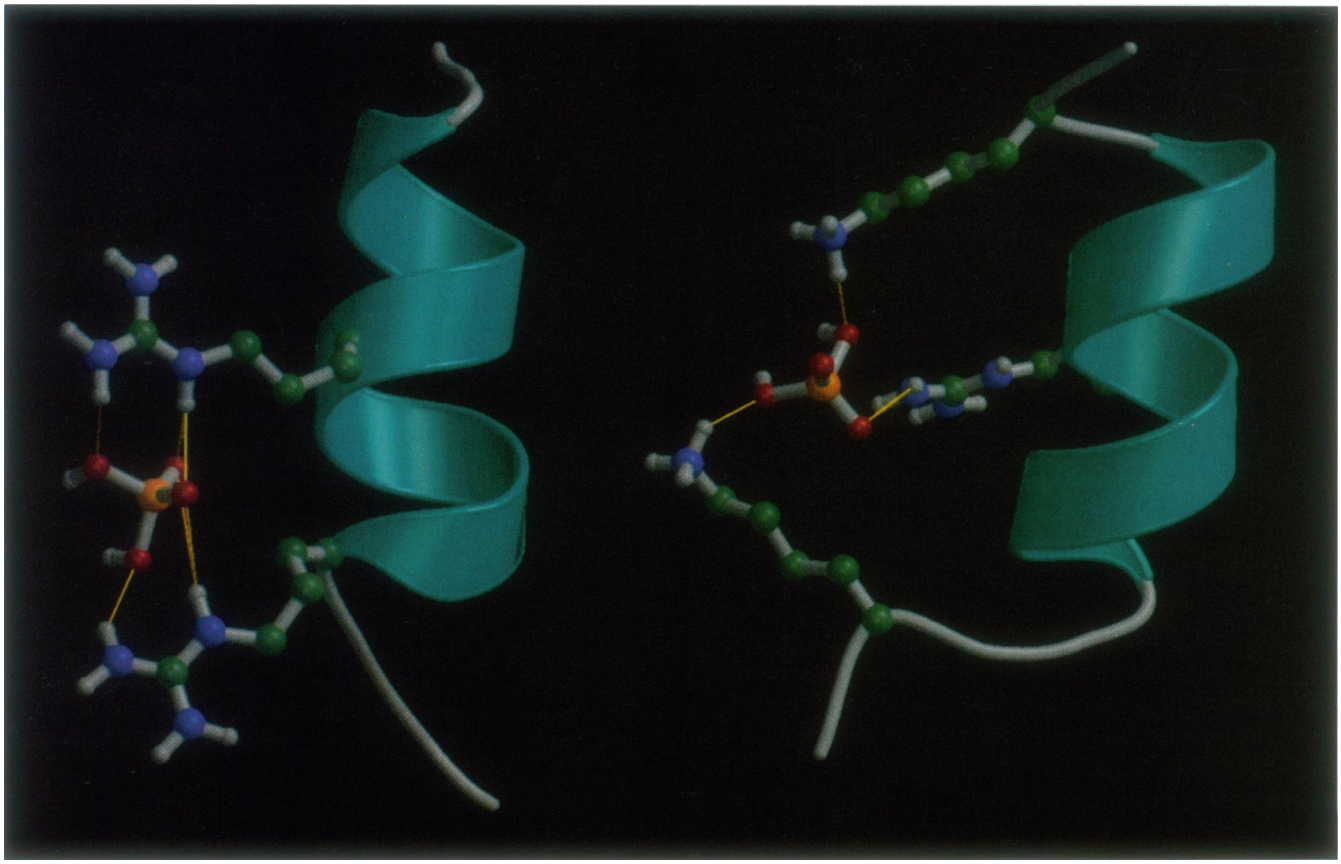

FIGURE 8 Hydrogen bonding between Pi and pep25 sidechains. (*Left*) Pi ion trapped between Arg-10 and Arg-14, (*right*) interaction between a Pi ion and Lys-7, Arg-14, and Lys-19. Plots were made with MOLSCRIPT (Kraulis, 1991) and Raster3D (Bacon and Anderson, 1988; Merritt and Murphy, 1994).

this happens a large number of times, an effective accumulation of charge at the cutoff is found. One can quite easily verify this by plotting radial distribution functions. In Fig. 9 we have plotted the RDF of the phosphorus atoms in Pi relative to each other for two simulations with different cutoffs and the RDF of Arg–CZ relative to each other in Sim 9Pi-D and Sim W. In the RDF of P for the 1.0 nm cutoff run there is a peak at 0.43 nm corresponding to hydrogen-bonded Pi molecules but also a broader and higher peak at 1.0 nm, which is exactly the cutoff distance. In the simulation with a 1.8 nm cutoff the peak at 0.43 nm is higher, and there is also a small second peak at 0.7 nm, corresponding to water-mediated hydrogen bonds. The peak at the cutoff distance is significantly lower than in the simulation with a cutoff distance of 1.0 nm; nevertheless, there is still an effect. These peaks at the cutoff distance are a well known artifact that arises from the use of cutoffs and can be rigorously avoided only by use of an appropriately chosen long-range electrostatic description (Berendsen, 1993). Therefore we used only the simulations with 1.8-nm long-range interactions for our analysis. In the RDF of Arg–CZ around each other we see a different effect. Without Pi there is a clear cutoff effect at 1.8 nm; with Pi there is only a small effect, and the peak at 0.7 nm is significantly higher and broader. This means that the Pi ions supply an effective screening of electrostatic interactions for the Arg–Arg interactions. This occurs in both Sim 9Pi-D and Sim 9Pi-R, as the RDF plots are very similar.

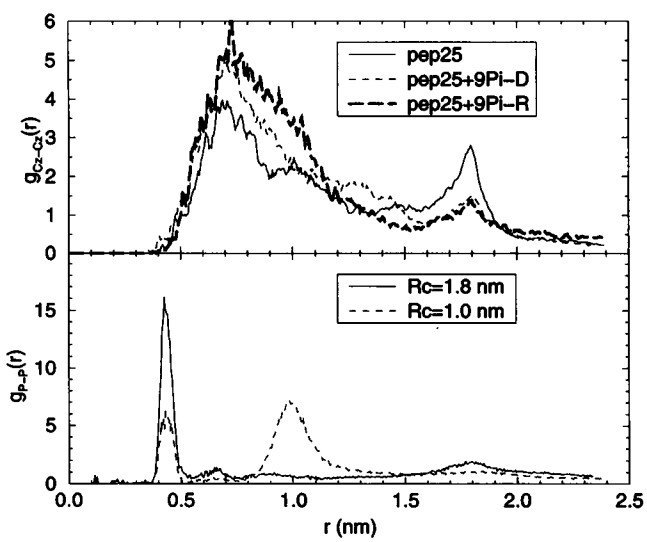

FIGURE 9 Radial distribution function of Pi–P around Pi-P in Sim 9Pi-D ($g_{P\text{-}P}$, *bottom*) and of Arg–CZ around Arg–CZ ($g_{CZ\text{-}CZ}$, *top*). Rc is the cutoff distance for Coulomb interactions. A running average over 0.015 nm was used to enhance clarity.

DISCUSSION

The 25 residue *N*-terminal fragment (pep25) of the coat protein of CCMV is a heavily charged peptide (+9). It is not visible in the electron density of the crystal structure (Speir et al., 1995) which was determined by use of the symmetry of the spherical virus coat that contains 180 icosahedrally arranged protein monomers. NMR has shown that the first eight residues of pep25 as part of the intact coat protein are mobile in empty viral capsids (without RNA), whereas the remainder of the peptide shows a measurable deviation from random coil $^1H_\alpha$ chemical shifts that is that of very similar to the isolated pep25 (van der Graaf et al., 1991). NMR and CD spectroscopy has revealed that the isolated peptide in solution has a tendency to form α-helices in the presence of phosphate ions (van der Graaf, 1992). In those experiments, different phosphate molecules were used as a model for RNA, to which pep25 is known to bind in the intact virus particle (Vriend et al., 1986). We performed MD simulations to study the interaction of monophosphate (Pi) ions with pep25 as a step toward a deeper understanding of pep25–RNA binding inside the virus particle. Although our study is not intended as structure refinement, we did compare the MD trajectories with experimental data to determine whether our results are meaningful in the biological context of the pep25-RNA interaction.

Three of our simulations, Sim W, Sim Pi4, and Sim Pi8, suffer from methodological problems. In Sim W the absence of counterions induces large repulsive forces among the nine charged residues. This problem is slightly reduced for Sim Pi4; the Pi4 molecule provides some electrostatic screening, but there still is a net charge of +5 in the system. Both Sim Pi4 and Sim Pi8 suffer from another problem: The absence of electrostatic screening from other ions forces pep25 and the phosphate group to maximize their interaction. In the case of Sim Pi8 all secondary structure in pep25 is lost after 1000 ps because of this effect. In Sim Pi4 this effect results in partial loss of α-helical structure, and the termini of pep25 fold around the Pi4 molecule. Although the conformations that occur in Sim W, Sim Pi4, and Sim Pi8 are not impossible, they do not seem very probable. The electrostatic screening problem is amplified by the use of a cutoff for electrostatic interactions. The cutoff effect is more serious for the Pi8 and Pi4 molecules than for either Pi or pep25, because the latter two molecules carry a higher charge than Pi and are more rigid than pep25; the charges are also more concentrated in Pi4 and Pi8 than in pep25. Both rigidity and charge density of Pi4 and Pi8 will probably induce a large effect on the surrounding water molecules. Another, minor, cutoff effect is observed in Sim 9Pi-D: When a Pi molecule is farther away than the cutoff distance from pep25, it no longer feels the attractive forces exerted by the positively charged residues. However, it may feel the repulsion of the Pi molecules that are still close to pep25. Therefore Pi ions that are far away from pep25 will have a low probability of approaching pep25. One can assess the extent of this effect by calculating the percentage of Pi that is outside the cutoff from pep25. By integration of the radial distribution function of Pi around pep25 from the cutoff to infinity we estimate that on average 3.5 of 9 Pi ions in Sim 9Pi-D do not see pep25. The result of this will be a reduced electrostatic screening of intrapeptide interactions.

Some methods, such as Ewald summation (Allen and Tildesley, 1987; Smith and Pettitt, 1991a) and particle–particle, particle–mesh (Hockney and Eastwood, 1981; Luty et al., 1994), are available to treat long-range electrostatic interactions in MD simulations, but none of these methods has, to our knowledge, been implemented on the message-passing parallel computers (Bekker et al., 1993; Berendsen et al., 1995) that we need to perform these long simulations. Therefore we are currently working on an improved long-range electrostatics treatment based on a Poisson solver (Berendsen, 1993) that can be implemented on our parallel computers. Until such a method becomes available we believe that our simulations are state of the art in the field of peptide simulations, because they cover a relatively long time (2.0 ns) and were performed with a relatively long cutoff of 1.8 nm. Although there still is a cutoff effect in Sim 9Pi-D, the radial distribution function of Arg–CZ around Arg–CZ (Fig. 9) shows that the positively charged Arg sidechains can approach one another more often owing to the electrostatic screening by the Pi ions. Fig. 9 also shows that the strength of the cutoff effect (the height of the peak at the cutoff length of 1.8 nm) is reduced by the addition of counterions in both Sim 9Pi-D and Sim 9Pi-R.

It should be noted that the pep25 concentration in our simulation is only a factor of 2.5 higher than in the NMR experiments that were done at a peptide concentration of 7 mM (corresponding to a peptide:water ratio of 1:7850, whereas we have 1:3264 in Sim 9Pi-D). This means that interactions among different pep25 molecules will often occur and also that interactions between pep25 and multiple phosphate molecules are very likely. The latter point is supported by experiments that show that an increase of the Pi concentration leads to larger α-helicity of pep25 (van der Graaf and Hemminga, 1991), which can be explained only by more interactions. With pep25 and Pi in a test tube there will always be Pi molecules in every direction around a pep25 molecule. This was also the case for Sim 9Pi-D and Sim 9Pi-R, for which one pep25 molecule was surrounded by nine Pi molecules. Hence, the sampling problem that is apparent in the other simulations does not affect Sim 9Pi-D. Therefore we conclude that these simulations are good enough for at least a qualitative interpretation of the data.

Correspondence with experimental data

We compared our simulation data of pep25 in Sim 9Pi-D with the relevant experimental data. The correspondence between CD spectroscopy and α-helicity in Sim 9Pi-D (Table 6) is remarkable. It should be kept in mind, however, that the result is biased by the starting structure, which contains a rather long α-helical part. The same reasoning

can also be applied to justify the results: Inasmuch as we remain relatively close to the starting structure (which was derived from experimental data) our simulation is sampling the configurational space close to a relevant structure.

Good qualitative agreement between measured and calculated $^1H_\alpha$ chemical shifts was found. The trend of the experimental data is reproduced (Fig. 3), although there is no quantitative agreement. In particular, the ten *N*-terminal residues deviate from the experimental data; part of this effect may be caused by binding of Pi to the Thr-2 and Thr-5 sidechains and to interactions of Pi with backbone atoms (Fig. 6). Because the experimental data show that this region of the peptide is in a random coil conformation (van der Graaf, 1992), the larger deviation indicates that the first 10 residues have too much secondary structure in Sim 9Pi-D. From the secondary structure plot (Fig. 5) and from the Pi binding plot (Fig. 6) it can be seen that the amount of secondary structure in the first 10 residues is reduced when no Pi is bound to it (after 1000 ps). This suggests that a longer simulation may improve the correspondence of $^1H_\alpha$ chemical shifts between experiment and simulation for this region of the peptide. As the Williamson–Asakura method for calculating chemical shifts (Williamson and Asakura, 1993) is an empirical method that is fitted on $^1H_\alpha$ atoms, we expect good correspondence between calculated and experimental data because we consider only $^1H_\alpha$ atoms. Furthermore, no aromatic residues are present in pep25, so no ring-current effects occur that could produce large $^1H_\alpha$ shifts. The only problem that can arise in the calculation of chemical shifts from structural data is the contribution of the local electric field, which does not take the solvent into account. Although it is hard to assess the strength of this effect, we believe that differences in $^1H_\alpha$ chemical shifts should be attributed primarily to different local conformation or insufficient sampling. Nevertheless, the qualitative agreement of experimental chemical shift data with our simulation data, together with the good agreement of α-helicity, demonstrates that the trajectory of Sim 9Pi-D is a physically meaningful data set, which is both valid and useful for further analysis. It seems that the measured $^1H_\alpha$ chemical shift δ values are closer to 0 when the random coil values of Merutka et al. (1995) are used than with those of Bundi and Wüthrich (1979), which may be the result of the difference in pH at which the random coil values were measured (pH 5.0 for Merutka et al. and pH 7.0 for Bundi and Wüthrich); pH 5.0 was also used for the experiments with pep25.

The results for Sim 9Pi-R are not nearly so good as those for Sim 9Pi-D. This means that the starting structure, including the positions of the ions relative to the peptides, is very important for the final result. Although some features of the chemical shift curve (Fig. 3), such as the peak at Leu-8, are reproduced very well in Sim 9Pi-R, the overall correspondance with experiment is not good; in particular, there is a strange peak at Ala-15. This peak corresponds to a dip in the α-helicity curve at Arg-14 (Fig. 2). When the peptide is α-helical there is substantial repulsion between the Arg-13/14 and Arg-18 sidechains if there is no electrostatic screening, as in the beginning of Sim 9Pi-R when the Pi ions are far away from the Arg residues. Breaking of the α-helix may be the simplest way to increase the distance between the positively charged residues, thereby facilitating water insertion into the backbone (DiCapua et al., 1990).

Interactions between Pi and pep25

All interactions between pep25 and Pi are largely electrostatic in nature. Nevertheless, it is useful to distinguish a number of different types of interaction: hydrogen bonds between Pi and pep25 backbone, hydrogen bonds with neutral-hydrogen-bond-forming sidechains, and ionic interaction between Pi and charged sidechains. The last-named type is essentially different because of its long-range nature. Direct hydrogen bonds between Pi and uncharged sidechains (Ser, Thr, and Asn) seem to be relatively strong once they have been formed (Fig. 7). However, in Sim 9Pi-R, for which such interactions are not formed initially, the Pi ions do not "find" the uncharged sidechains in the 2.0-ns simulation. Thus we cannot draw any conclusions on the amount of Pi around these sidechains, because our simulations have not converged. For Pi binding to charged Lys and Arg sidechains, in contrast, we do find converged RDF plots (see Figs. 7 and 9). We also plotted RDFs for the first and last nanoseconds of our simulations (data not shown). In this case there was no convergence between the simulations and no convergence between first and last nanoseconds of our simulations either. From these findings we conclude that the 2.0-ns simulation is the smallest simulation time that is long enough for sampling of charge–charge configurations. One can expect that the sampling will be worse when fewer ions are used and vice versa. To obtain a proper sampling of the interactions between Pi and the neutral sidechains probably requires a simulation time that is an order of magnitude larger than the 2.0-ns time that we used. Another feature of the RDFs is that both Arg and Lys have a broad distribution of Pi (Fig. 7) and a large secondary peak, corresponding to water-mediated hydrogen bonds, which is virtually absent in the other RDFs. The observation that Pi interacts with pep25 mostly through water-mediated hydrogen bonds is similar to what was found in a simulation study of Enkaphalin in 1 M acetate solution (Smith et al., 1993).

Binding of Pi to pep25 involves some kind of cooperativity: Once a Pi ion is bound, to either a sidechain or a backbone atom, it very often binds to more than one residue simultaneously or makes multiple hydrogen bonds with the same residue. Despite the high charge of +9 on pep25, only a small number of Pi ions bind to pep25; apparently the desolvation of both Pi and pep25 is energetically unfavorable.

The promotion of α-helix content by Pi in Sim 9Pi-D is primarily an effect of electrostatic screening. The experimental results can also be explained this way: Increasing the salt concentration increases the charge screening effect. The small difference between phosphates and other salts is that they sometimes, but certainly not often, bind through direct

hydrogen bonds. One effect of longer phosphate molecules is that the repulsion between negatively charged groups cannot increase their distance, and therefore screening is increased even more. It is likely that the possibility of making several ionic contacts simultaneously, together with the higher rigidity of the longer phosphate chains, meaning less entropy loss on binding, will make binding of oligophosphates more favorable than binding of Pi ions. It seems plausible that the same reasoning can be applied to binding of pep25 to RNA.

α-Helix initiation

It has been suggested that Gln-12 and Thr-9 are involved in the primary loop formation of the α-helical structure. This would involve a stable hydrogen bond between Gln-12 and Thr-9 (van der Graaf et al., 1992). We did indeed find hydrogen bonds between the Gln-12 sidechain and backbone and the Thr-9 sidechain. These hydrogen bonds were not present in our starting conformation but were formed during the simulation. Interestingly, a hydrogen bond between Thr-9–CO and Arg-13–NH was found from 1300 to 2000 ps simultaneously with the Thr-9–Oγ to Gln-12–NH hydrogen-bond, whereas neither the DSSP program (Kabsch and Sander, 1983; Fig. 5) nor the Ramachandran-angle-based criterion of Hirst and Brooks (1994; Fig. 2) determined Thr-9 to be in an α-helical conformation. Arg-10, however, is in α-helical conformation from 1340 ps to the end of the simulation. The ϕ angle of Arg-10 changes from +60 to −60, entering the α-helical region of the Ramachandran plot shortly after the Thr-9–CO to Arg-13–NH hydrogen bond is formed. In contrast, the Thr-9 residue is found to be in the β-sheet region of the Ramachandran plot with a positive ψ angle. Therefore we conclude that indeed Thr-9 and Gln-12 are involved in a start of the α-helix and that the α-helix cannot extend in the *N*-terminal direction because of the "wrong" ϕ/ψ angles of residue Thr-9. A nuclear Overhauser–effect connectivity $d_{\alpha N}$ between Thr-9 and Ala-11 that was found by NMR experiments (van der Graaf, 1992), is also present in Sim 9Pi-D: Thr-9–C_α and Ala-11–H are never more than 0.4 nm apart.

CONCLUSIONS

Of the five MD simulation that we performed, Sim 9Pi-D is the best one in methodological terms. We have shown that for this simulation there is at least qualitative agreement with experimental $^1H_\alpha$ chemical shift data and α-helicity from CD experiments. The interaction between Thr-9 and Gln-12 that was suggested on the basis of chemical shifts was indeed found. Because of this interaction the ϕ/ψ angles of residue Thr-9 are not α-helical, thereby prohibiting α-helix extension in the *N*-terminal direction. The hydrogen bond between Thr-9 and Gln-12 probably induces a transition of Arg-10 to the α-helical region of the Ramachandran plot. In our simulation the region from residue Arg-10 through Lys-19 is the α-helical part, which corresponds very well to experimental results (van der Graaf, 1992). The control simulation starting from random Pi positions (Sim 9Pi-R) shows that in 2.0 ns the charge–charge interactions can be sampled adequately, although the overall equilibration of phosphate distribution is not achieved. The latter finding may imply that the interactions of Pi with neutral sidechains in Sim 9Pi-D are exaggerated because of the docking procedure. The interaction of Pi with charged sidechains is very often mediated by water molecules; apparently the complete desolvation of two charged groups is energetically unfavorable.

We thank Dr. Janez Mavri for assistance with the ab initio calculations and Dr. Gert Vriend and Dr. Tjeerd Schaafsma for valuable discussions. D. v. d. S. acknowledges support from the Netherlands Foundation for Chemical Research, with financial aid from the Netherlands Organization for Scientific Research.

REFERENCES

Allen, M. P., D. J. Tildesley. 1987. *Computer Simulations of Liquids.* Oxford Science Publications, Oxford.

Bacon, D. J., W. F. Anderson. 1988. A fast algorithm for rendering space-filling molecule pictures. *J. Molec. Graph.* 6:219–220.

Bancroft, J. B., E. Hiebert. 1967. Formation of an infectious nucleoprotein from protein and nucleic acid isolated from a small spherical virus. *Virology.* 32:354–356.

Bekker, H., H. J. C. Berendsen, E. J. Dijkstra, S. Achterop, R. van Drunen, D. van der Spoel, A. Sijbers, H. Keegstra, B. Reitsma, and M. K. R. Renardus. 1993. Gromacs: a parallel computer for molecular dynamics simulations. *In Physics Computing 92.* R. A. de Groot and J. Nadrchal, editors. World Scientific, Singapore. 252–256.

Berendsen, H. J. C. 1993. Electrostatic interactions. *In Computer Simulation of Biomolecular Systems* W. F. van Gunsteren, P. K. Weiner, and A. J. Wilkinson, editors. ESCOM, Leiden, The Netherlands. 161–181.

Berendsen, H. J. C., J. P. M. Postma, A. DiNola, and J. R. Haak. 1984. Molecular dynamics with coupling to an external bath. *J. Chem. Phys.* 81:3684–3690.

Berendsen, H. J. C., J. P. M. Postma, W. F. van Gunsteren, and J. Hermans. 1981. Interaction models for water in relation to protein hydration. *In Intermolecular Forces.* B. Pullman, editor. D. Reidel Publishing Company, Dordrecht, The Netherlands. 331–342.

Berendsen, H. J. C., D. van der Spoel, and R. van Drunen. 1995. GROMACS: a message-passing parallel molecular dynamics implementation. *Comput. Phys. Commun.* 91:43–56.

Besler, B. H., K. M. Merz, Jr., and P. A. Kollman. 1990. Atomic charges derived from semiempirical methods. *J. Comp. Chem.* 11:431–439.

Brooks, C. L. III. 1993. Molecular simulations of peptide and protein unfolding: in quest of a molten globule. *Curr. Opin. Struct. Biol.* 3:92–98.

Brooks, C. L. III, and L. Nilsson. 1993. Promotion of helix formation in peptides dissolved in alcohol and water-alcohol mixtures. *J. Am. Chem. Soc.* 115:11034–11035.

Bundi, A., and K. Wüthrich. 1979. ^{1}H-NMR parameters of the common amino acid residues measured in aqueous solutions of the linear tetrapeptides H–Gly–Gly–X–L–Ala–OH. *Biopolymers.* 18:285–297.

Caflisch, A., and M. Karplus. 1994. Molecular dynamics studies of protein and peptide folding and unfolding. *In The Protein Folding Problem and Tertiary Structure Prediction.* K. M. Merz, Jr., and S. M. Le Grand, editors. Birkhäuser, Boston, MA. 193–230.

Case, D. A. 1995. Calibration of ring-current effects in proteins and nucleic acids. *J. Biomol. NMR.* 6:341–346.

Clarage, J. B., and G. N. Philips, Jr. 1994. Cross-validation tests of time-averaged molecular dynamics refinements for determination of protein structures by x-ray crystallography. *Acta Crystallogr. D.* 50:24–36.

Dasgupta, R., and P. Kaesberg. 1982. Complete nucleotide sequence of the coat protein messenger RNAs of brome mosaic virus and cowpea chlorotic mottle virus. *Nucl. Acid. Res.* 10:703–713.

Daura, X., B. Oliva, E. Querol, F. X. Avilés, and O. Tapia. 1996. On the sensitivity of MD trajectories to changes in water-protein interaction parameters: the potato carboxypeptidase inhibitor in water as a test case for the GROMOS force field. *Proteins: Struct. Funct. Gen.* 25:89–103.

de Dios, A. C., J. G. Pearson, and E. Oldfield. 1995. Secondary and tertiary structural effects on protein NMR chemical shifts: an ab initio approach. *Science.* 260:1491–1496.

de Loof, H., L. Nilsson, and R. Rigler. 1992. Molecular dynamics simulations of galanin in aqueous and nonaqueous solution. *J. Am. Chem. Soc.* 114:4028–4035.

DiCapua, F. M., S. Swaminathan, and D. L. Beveridge. 1990. Theoretical evidence for destabilization of an α helix by water insertion: molecular dynamics of hydrated decaalanine. *J. Am. Chem. Soc.* 112:6768–6771.

Fennen, J., A. E. Torda, and W. F. van Gunsteren. 1995. Structure refinement with molecular dynamics and Boltzmann-weighted ensemble. *J. Biomol. NMR.* 6:163–170.

Frisch, M. J., G. W. Trucks, H. B. Schlegel, P. M. W. Gill, B. G. Johnson, M. W. Wong, J. B. Foresman, M. A. Robb, M. Head-Gordon, E. S. Replogle, R. Gomperts, J. L. Andres, K. Raghavachari, J. S. Binkley, C. Gonzalez, R. L. Martin, D. J. Fox, D. J. Defrees, J. Baker, J. J. P. Stewart, and J. A. Pople. 1993. *Gaussian 92/DFT, Revision G. I.* Gaussian, Inc., Pittsburgh, PA.

Hirst, J. D., and C. L. Brooks III. 1994. Helicity, circular dichroism and molecular dynamics of proteins. *J. Mol. Biol.* 243:173–178.

Hockney, R. W., and J. W. Eastwood. 1981. *Computer Simulation Using Particles.* McGraw-Hill Book Company, New York.

Kabsch, W., and C. Sander, 1983. Dictionary of protein secondary structure: pattern recognition of hydrogen-bonded and geometrical features. *Biopolymers.* 22:2577–2637.

Kovacs, H., A. E. Mark, J. Johansson, and W. F. van Gunsteren. 1995. The effect of environment on the stability of an integral membrane helix: molecular dynamics simulations of surfactant protein C in chloroform, methanol and water. *J. Mol. Biol.* 247:808–822.

Kraulis, P. J. 1991. MOLSCRIPT: a program to produce both detailed and schematic plots of protein structures. *J. Appl. Crystallogr.* 24:946–950.

Lee, W. K., and E. W. Prohofsky. 1982. A molecular dynamics study of the solvation of a sodium ion bound to dihydrogen phosphate ion. *Chem. Phys. Lett.* 85:98–102.

Luty, B. A., M. E. Davies, I. G. Tironi, and W. F. van Gunsteren. 1994. A comparison of particle–particle, particle–mesh and Ewald methods for calculating electrostatic interactions in periodic molecular systems. *Mol. Sim.* 14:11–20.

Mark, A. E., and W. F. van Gunsteren. 1992. Simulation of the thermal denaturation of hen egg white lysozym: trapping the molten globule state. *Biochemistry.* 31:7745–7748.

Merritt, E. A., and M. E. P. Murphy. 1994. Raster3D version 2.0: a program for photorealistic molecular graphics. *Acta Crystallogr. D.* 50:869–873.

Merutka, G., H. J. Dyson, and P. E. Wright. 1995. "Random coil" ^{1}H chemical shifts obtained as a function of temperature and trifluoroethanol concentration for the peptide series GGXGG. *J. Biomol. NMR.* 5:14–24.

MSI (1994). *QUANTA 3.0.* Molecular Simulations, Inc., York, U.K.

Ösapay, K., and D. A. Case. 1991. A new analysis of proton chemical shifts. *J. Am. Chem. Soc.* 113:9436–9444.

Ösapay, K., and D. A. Case. 1994. Analysis of proton chemical shifts in regular secondary structure of proteins. *J. Biomol. NMR.* 4:215–230.

Pearson, J. G., J. F. Wang, J. L. Markley, H. B. Le, and E. Oldfield. 1995. Protein structure refinement using carbon-13 nuclear magnetic resonance spectroscopic chemical shifts and quantum chemistry. *J. Am. Chem. Soc.* 117:8823–8829.

Ryckaert, J. P., G. Ciccotti, and H. J. C. Berendsen. 1977. Numerical integration of the cartesian equations of motion of a system with constraints; molecular dynamics of *n*-alkanes. *J. Comp. Phys.* 23:327–341.

Sijpkes, A. H., G. van der Kleut, and S. C. Gill. 1993. Urea-diketopiperazine interactions: a model for urea induced denaturation of proteins. *Biophys. Chem.* 46:171–177.

Smith, P. E., G. E. Marlow, and B. Montgomery Pettitt. 1993. Peptides in ionic solutions: A simulation study of a bis(penicillamine) enkaphalin in sodium acetate solution. *J. Am. Chem. Soc.* 115:7493–7498.

Smith, P. E., and B. M. Pettitt. 1991a. Peptides in ionic solutions: a comparison of the Ewald and switching function techniques. *J. Chem. Phys.* 95:8430–8441.

Smith, P. E., and B. M. Pettitt. 1991b. Effects of salt on the structure and dynamics of the bis(penicillamine) enkaphalin zwitterion: a simulation study. *J. Am. Chem. Soc.* 113:6029–6037.

Speir, J. A., S. Munshi, G. Wang, T. S. Baker, and J. E. Johnson. 1995. Structures of the native and swollen forms of cowpea chlorotic mottle virus determined by x-ray crystallography and cryo-electron microscopy. *Structure.* 3:63–78.

Spera, S., and A. Bax. 1991. Empirical correlation between protein backbone conformation and C_α and C_β ^{13}C nuclear magnetic resonance chemical shifts. *J. Am. Chem. Soc.* 113:5490–5492.

ten Kortenaar, P. B. W., J. Krüse, M. A. Hemminga, and G. I. Tesser. 1986. Synthesis of an arginine rich fragment of a viral coat protein using guanidium functions exclusively. *Int. J. Pept. Protein Res.* 27:401–413.

Timasheff, S. N. 1992. Solvent effects on protein stability. *Curr. Opin. Struct. Biol.* 2:35–39.

Tirado-Rives, J., and W. L. Jorgensen. 1993. Molecular dynamics simulations of the unfolding of apomyoglobin in water. *Biochemistry.* 33:4175–4184.

van Buuren, A. R., and H. J. C. Berendsen. 1993. Molecular dynamics simulation of the stability of a 22 residue alpha-helix in water and 30% trifluoroethanol. *Biopolymers.* 33:1159–1166.

van Buuren, A. R., S. J. Marrink, and H. J. C. Berendsen. 1993. A molecular dynamics study of the decane/water interface. *J. Phys. Chem.* 97:9206–9212.

van der Graaf, M. 1992. Conformation of the RNA-binding *N*-terminus of the coat protein of cowpea chlorotic mottle virus. Ph.D. dissertation. Wageningen Agricultural University, Wageningen, The Netherlands.

van der Graaf, M., and M. A. Hemminga. 1991. Conformational studies on a peptide representing the RNA-binding *N*-terminus of a viral coat protein using circular dichroism and NMR spectroscopy. *Eur. J. Biochem.* 201:489–494.

van der Graaf, M., G. J. A. Kroon, and M. A. Hemminga. 1991. Conformation and mobility of the RNA-binding *N*-terminal part of the intact coat protein of cowpea chlorotic mottle virus. A two dimensional nuclear magnetice resonance study. *J. Mol. Biol.* 220:701–709.

van der Graaf, M., R. M. Scheek, C. C. van der Linden, and M. A. Hemminga. 1992. Conformation of a pentacosapeptide representing the RNA-binding *N*-terminus of cowpea chlorotic mottle virus coat protein in the presence of oligophosphates: a two-dimensional proton nuclear magnetic resonance and distance geometry study. *Biochemistry.* 31: 9177–9182.

van der Spoel, D., A. R. van Buuren, E. Apol, P. J. Meulenhoff, D. P. Tieleman, A. L. T. M. Sijbers, R. van Drunen, and H. J. C. Berendsen. 1996. *Gromacs User Manual version 1.3.* Nijenborgh 4, 9747 AG Groningen, The Netherlands. Internet: http://rugmd0.chem.rug.nl/~gmx.

van Gunsteren, W. F., and H. J. C. Berendsen. 1987. *Gromos-87 manual.* Biomos BV, Nijenborgh 4, 9747 AG Groningen, The Netherlands.

van Schaik, R. C., H. J. C. Berendsen, A. E. Torda, and W. F. van Gunsteren. 1993. A structure refinement method based on molecular dynamics in 4 spatial dimensions. *J. Mol. Biol.* 234:751–762.

Vriend, G., M. A. Hemminga, B. J. M. Verduin, J. L. de Wit, and T. J. Schaafsma. 1981. Segmental mobility involved in protein-RNA interaction in cowpea chlorotic mottle virus. *FEBS Lett.* 134:167–171.

Vriend, G., B. J. M. Verduin, and M. A. Hemminga. 1986. Role of the *N*-terminal part of the coat protein in the assembly of cowpea chlorotic mottle virus. *J. Mol. Biol.* 191:453–460.

Vriend, G., B. J. M. Verduin, M. A. Hemminga, and T. J. Schaafsma. 1982. Mobility involved in protein-RNA interaction in spherical plant viruses, studied by nuclear magnetic resonance spectroscopy. *FEBS Lett.* 145: 49–52.

Williamson, M. P., and T. Asakura. 1993. Empirical comparisons of models for chemical-shift calculation in proteins. *J. Magn. Reson. Ser. B.* 101:63–71.